

Chiral and deconfinement transition from correlation functions: SU(2) vs. SU(3)

Christian S. Fischer^{1,2}, Axel Maas^{3 a}, and Jens A. Müller^{1 b}

¹ Institut für Kernphysik, Technische Universität Darmstadt, Schlossgartenstraße 9, D-64289 Darmstadt, Germany

² GSI Helmholtzzentrum für Schwerionenforschung GmbH, Planckstr. 1 D-64291 Darmstadt, Germany

³ Institut für Physik, Karl-Franzens Universität Graz, Universitätsplatz 5, A-8010 Graz, Austria

Received: date / Revised version: date

Abstract. We study a gauge invariant order parameter for deconfinement and the chiral condensate in SU(2) and SU(3) Yang-Mills theory in the vicinity of the deconfinement phase transition using the Landau gauge quark and gluon propagators. We determine the gluon propagator from lattice calculations and the quark propagator from its Dyson-Schwinger equation, using the gluon propagator as input. The critical temperature and a deconfinement order parameter are extracted from the gluon propagator and from the dependency of the quark propagator on the temporal boundary conditions. The chiral transition is determined using the quark condensate as order parameter. We investigate whether and how a difference in the chiral and deconfinement transition between SU(2) and SU(3) is manifest.

PACS. 12.38.Aw – 12.38.Lg – 11.15.Ha – 12.38.Mh – 25.75.Nq

1 Introduction

Two of the most characteristic features of QCD are at the same time two of the most elusive ones: Confinement and chiral symmetry breaking. Of particular interest is the dependency of these phenomena on temperature and density. For vanishing current quark masses chiral symmetry gets restored by a phase transition above a critical temperature. On the other hand in the limit of infinitely heavy quarks a phase transition from a confining phase to a deconfined phase takes place. Of course, in full QCD with physical quarks none of the aforementioned limits is appropriate. Indeed, at zero chemical potential the would-be order parameters for both transitions show a rapid change signaling a well-marked cross-over region [1]. Furthermore it seems remarkable that the temperature ranges for both cross-overs are notable close to each other [2, 3, 4]. This is in contrast to *e.g.* the case of adjoint quarks where both temperatures differ by a factor of almost eight [5].

Thus, it warrants to investigate the chiral and deconfinement transition for fundamental quarks closely, to eventually understand both properties. To avoid the problems involved with dynamical quarks, a useful laboratory is the quenched approximation where only valence quarks are present. In this case the deconfinement transition can be cleanly defined by usage of the Polyakov-loop as order parameter, and both the chiral restoration and deconfinement temperature coincide within available accuracy [6].

Useful tools to address these questions are the so-called dual observables [7, 8, 9, 10, 11, 12, 13, 14, 15, 16, 17]. These are obtained by modifying the temporal boundary conditions of the valence (test) quarks, without altering the dynamics of the theory¹. Dual observables are sensitive to the spectral properties of the Dirac operator, and thus do encode both the confinement and the chiral properties of quarks. In particular, they are not only able to distinguish the low-temperature from the high-temperature phase, but also phases where chiral symmetry is broken but confinement is no longer present [12].

Dual observables have been first defined using lattice gauge theory [8], but have turned out to be quite expensive to determine. In particular, the large distances characteristic of confining physics and the small masses relevant to chiral symmetry are hard to reach. On the other hand, it is also possible to determine dual quantities using functional methods [13, 17]. In this case, there is no limit neither on distance nor on the quark masses. The challenge is, however, that truncations are necessary. In this work we combine the best of both worlds by a combination of lattice and continuum methods [13, 14, 19].

The goal of our study is twofold. On the one hand we investigate (potentially gauge-dependent) mechanisms linking deconfinement and chiral symmetry restoration. The study presented in this work in particular highlights the role of the longitudinal, electric part of the Landau gauge gluon propagator in this respect. On the other hand

^a *e-mail:* axelmaas@web.de

^b *e-mail:* jens.mueller@physik.tu-darmstadt.de

¹ Such an alteration would correspond to the introduction of an imaginary chemical potential [18] as discussed in Ref. [17].

our study serves as an important intermediate step towards an analysis of the QCD phase diagram at non-vanishing chemical potential. Due to the notorious sign problem of lattice QCD in that realm there is great demand for other methods beyond model calculations. Functional methods like Dyson-Schwinger equations [20, 21] and the functional renormalization group [22] are ready to fill this gap. To provide for meaningful results at non-zero chemical potential it is, however, first necessary to gain as much insight as possible into the fidelity of truncations at zero chemical potential, where one can compare with the results from lattice QCD. As a result of this work we find a clear (gauge-invariant) signal for the deconfinement transition from the dressed Polyakov-loop determined from the Dyson-Schwinger equations in agreement with the information we extract from the lattice gluon propagator.

This paper is organised as follows: Our method to determine the magnetic and electric part of the Landau gauge gluon propagator on the lattice are discussed in section 2. Though the gluon propagator is gauge-dependent, it is found that it can be used to obtain gauge-invariant properties, like the critical temperature. The gluon propagator is also one of the key ingredients into the Dyson-Schwinger equation for the quark propagator. In principle the gluon propagator could be obtained using Dyson-Schwinger equations [19, 23, 24, 25], but this turns out to be a formidable task [19]. Instead we use our result from lattice gauge theory as input, as described in section 3. From the Landau gauge quark propagator we then extract the gauge-invariant order parameters for the chiral and deconfinement transition. This procedure has been used previously in [13, 14]. However, the then available lattice data [19] for the gluon propagator have been very coarse on the temperature axis, and only available for SU(2). We expand here to a much finer grid in the temperature domain, while at the same time employing much larger physical volumes on the lattice. Preliminary results of these calculations can be found in [26]. In addition, we study the physical case of SU(3)². The results are summarized in section 4.

2 The gluon propagator from lattice calculations

2.1 Simulation details

To determine the gluon propagator between zero and roughly two times the critical temperature ($T_c = 277$ MeV for SU(2) and $T_c = 303$ MeV for SU(3)), lattice gauge theory implementing the Wilson action is used, details can be found in [19, 28]. Details of the simulation parameters can be found in appendix A, in particular its table 1. There also systematic errors will be discussed. This investigation extends previous works in the same temperature range [19, 29], and at higher temperatures [30].

² First explorative studies of the gluon propagator in the unquenched case can be found in [27].

At finite temperature, the Landau gauge gluon propagator $D_{\mu\nu}$ is described by two independent dressing functions, D_T and D_L ,

$$\begin{aligned} D_{\mu\nu}^{ab}(p) &= P_{\mu\nu}^T(p) D_T^{ab}(\omega_p^2, \mathbf{p}^2) + P_{\mu\nu}^L D_L^{ab}(\omega_p^2, \mathbf{p}^2) \\ P_{\mu\nu}^T(p) &= (1 - \delta_{\mu 0})(1 - \delta_{\nu 0}) \left(\delta_{\mu\nu} - \frac{p_\mu p_\nu}{p^2} \right) \\ P_{\mu\nu}^L(p) &= P_{\mu\nu}(p) - P_{\mu\nu}^T(p), \end{aligned}$$

where $P_{\mu\nu}^T$ and $P_{\mu\nu}^L$ are projectors transverse and longitudinal to the heat bath. The color-dependency of the propagator has been evaluated in lattice gauge theory, and has always been found to be consistent with a color-diagonal propagator [28]. Thus there remain two scalar functions $D_T = Z_T/p^2$ (transverse to the heat bath's four-velocity, chromomagnetic) and $D_L = Z_L/p^2$ (parallel to the heat bath's four-velocity, chromoelectric), with $Z_T = Z_L$ at zero temperature, for the description of the gluon. Here p denotes always the four-momentum with $p^2 = \omega_p^2 + \mathbf{p}^2$, which coincides with the three-momentum for the soft modes $\omega_p = 0$. Only this soft mode will be discussed in detail here. The hard modes are discussed separately in appendix B, and found to be very well approximated by $D(\omega_p^2, \mathbf{p}^2) = D(0, \omega_p^2 + \mathbf{p}^2)$.

The gluon propagator, as the gluon itself, is only well-defined in a fixed gauge. For the purpose of calculating gauge-invariant quantities the choice of gauge is irrelevant, but since gauge-dependent intermediate results will be transferred from one method to another here, a non-perturbatively unambiguous definition of the gauge seems necessary. We choose here the minimal or average- B Landau gauge [31, 32]. For the discussions of other choices see [32, 33, 34, 35]. However, the gluon propagator at the volumes employed here is depending only marginally on this choice [32, 34]. In particular, the effect is likely only of the same order as other systematic effects of the present calculations. Therefore, it can also be used for similar other calculations, independent of the particular choice between all non-perturbative realizations of the Landau gauge. The methods used to fix this gauge at finite temperature can be found in [19] for SU(2), and the extension used to address SU(3) in [36]. In [19, 28] also the methods used to determine the gluon propagator are presented. Note that the method to determine the value of the gluon fields employed in general and in particular in [19] is only applicable to configurations with positive real part of the Polyakov loop [29]. Therefore, only such configurations have to be included in the Monte-Carlo average which satisfy this condition. This is performed by filtering at all temperatures for this condition.

In addition to the gluon we determine the ghost propagator D_G , related to its dressing function by

$$D_G(p) = \frac{G(p)}{p^2} \quad (1)$$

and found previously to be color-diagonal [28]. In contrast to the gluon propagator, the ghost is expected to depend significantly on the gauge choice for momenta $p < 1$ GeV

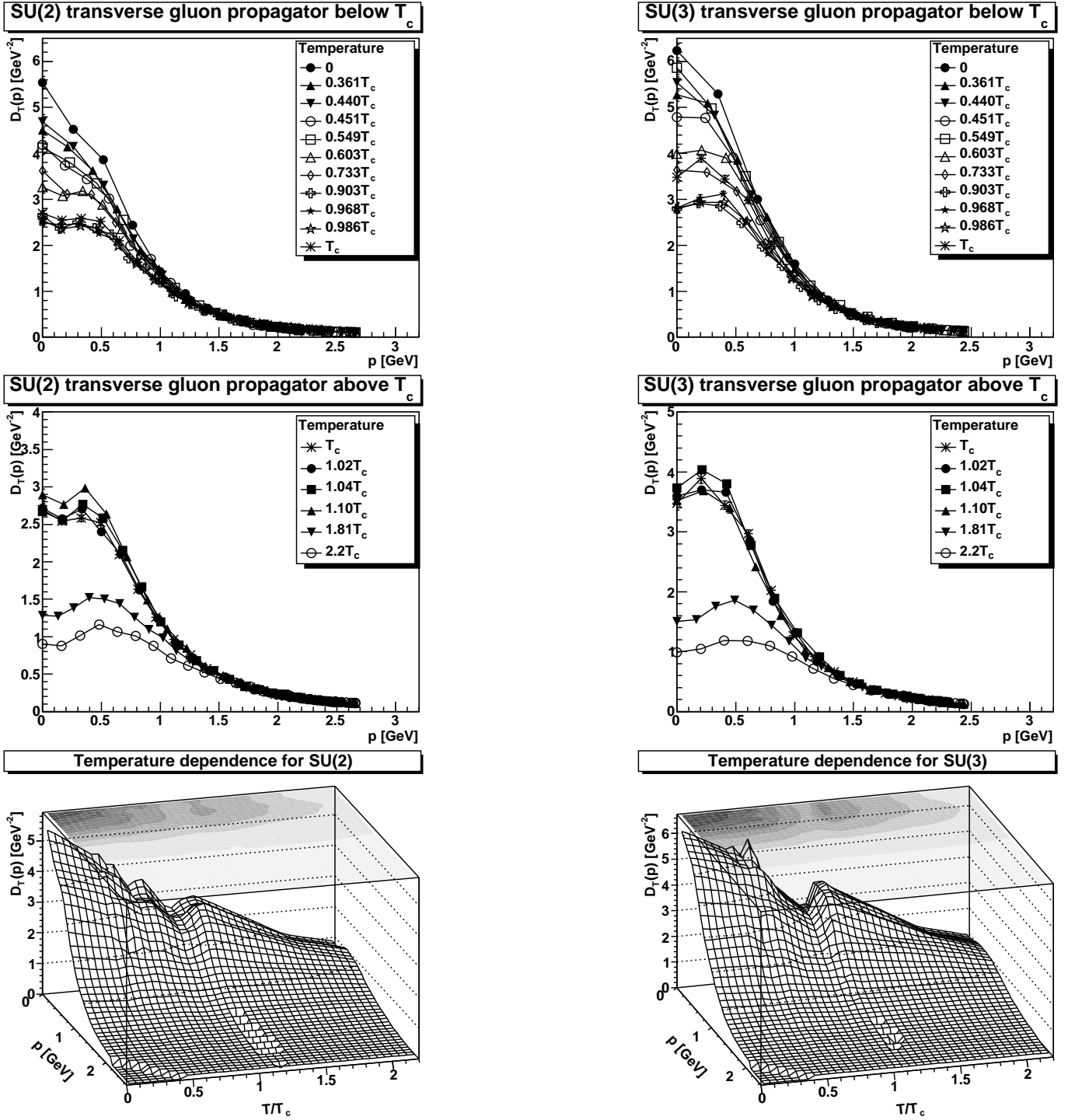


Fig. 1. The (soft mode of the) transverse part D_T of the gluon propagator at temperatures below (top panel) and above (middle panel) the phase transition. The bottom panel shows both results together. On the left results for SU(2) and on the right results for SU(3) are shown. Lines are drawn to guide the eye. Momenta here and hereafter are aligned along the x -axis.

[32,33,34]. Here, the only reason for its investigation is to study the prediction of functional methods [19] that the gauge-fixing dynamics, which is essentially given by the ghost propagator, is insensitive to the phase transition. This is indeed the case as already indicated by the results

of Ref. [19] and further confirmed by our results for the ghost discussed in appendix C.

All results presented are renormalized such that at 2 GeV the dressing functions in all cases equal 1, for convenience. The renormalization factor is determined by the average value of the propagators at the closest momen-

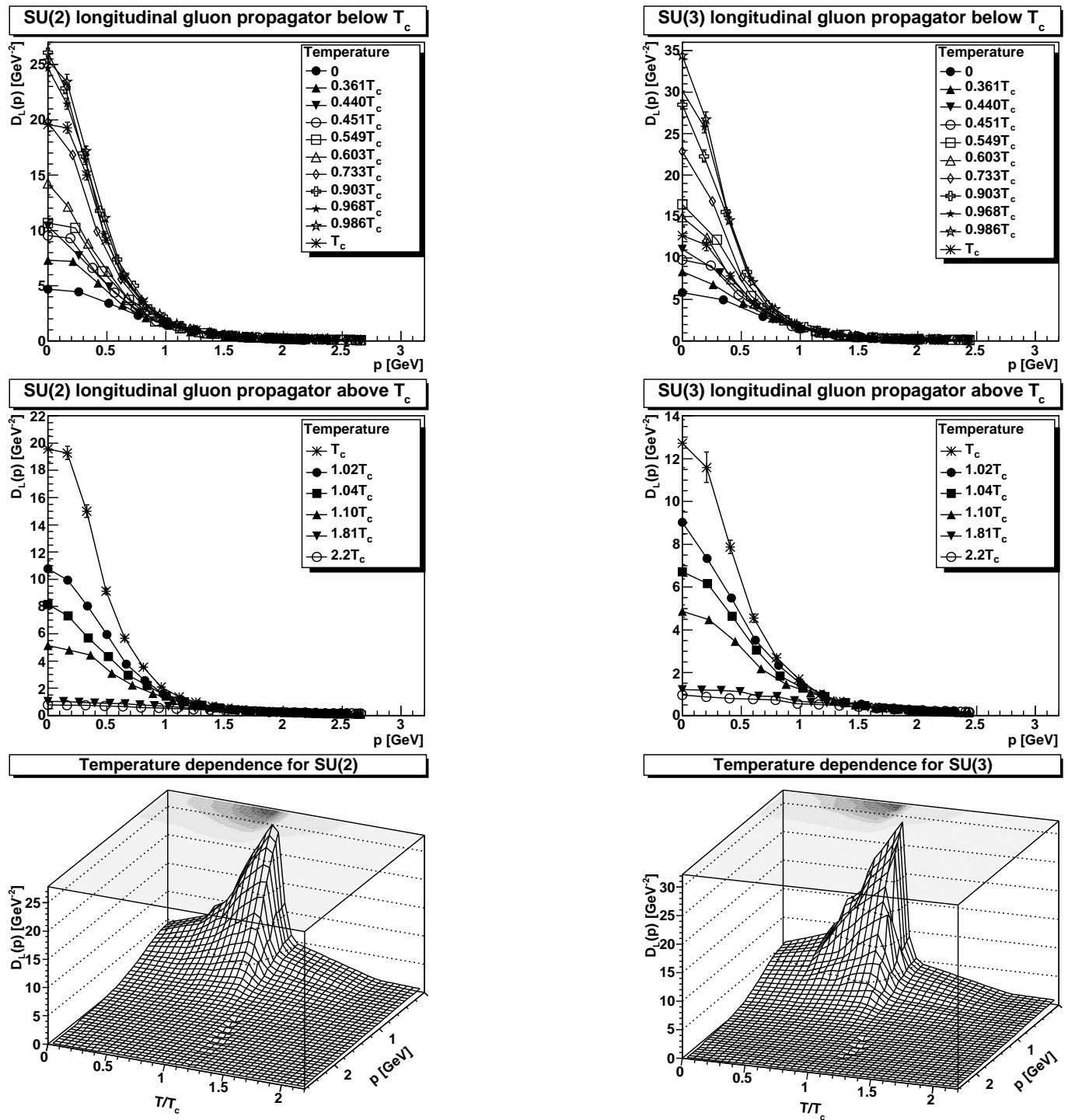


Fig. 2. The (soft mode of the) longitudinal part D_L of the gluon propagator at temperatures below (top panel) and above (middle panel) the phase transition. The bottom panel shows both results together. On the left results for SU(2) and on the right results for SU(3) are shown. Lines are drawn to guide the eye.

tum values above and below 2 GeV in the x - y -plane. This procedure entails that the renormalization constants are temperature-dependent. They vary by about 10% for the transverse gluon and the ghost, but by up to 50% for the longitudinal gluon in the investigated temperature and discretization range.

2.2 Results

The finite-temperature results for the transverse part D_T of the gluon propagator are shown in figure 1. In the left panel we display the results for SU(2) and in the right panel corresponding results for SU(3). The temper-

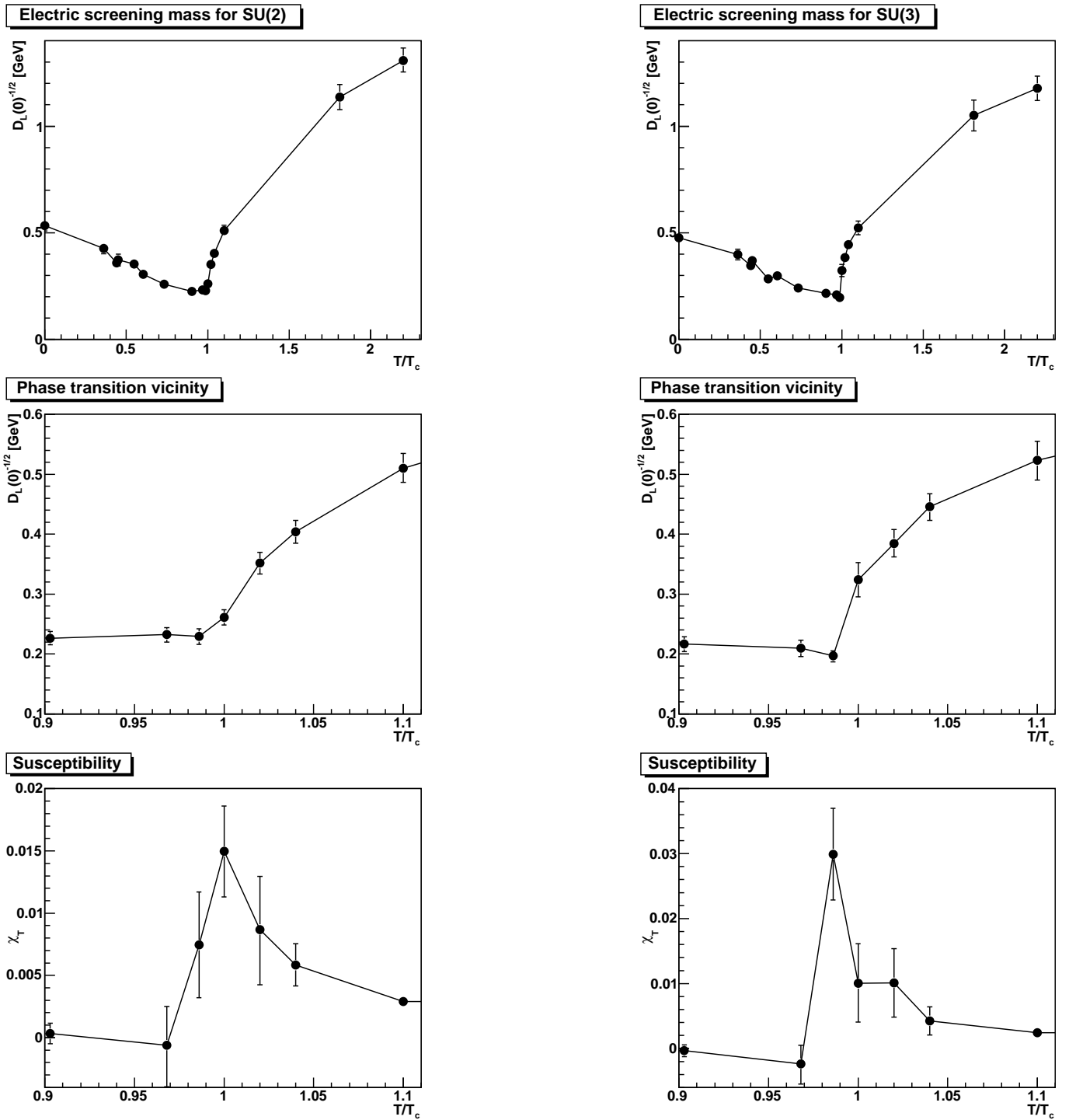


Fig. 3. The electric screening mass as a function of temperature (top panel), and zoomed in the phase transition region (middle panel). The corresponding susceptibility $\chi_T = \partial D_L(0)^{-1/2} / \partial T$ is shown in the bottom panel. On the left results for SU(2) and on the right results for SU(3) are shown. Note the respective different range for SU(2) and SU(3) for the susceptibility. Lines are drawn to guide the eye.

ature behaviour of each momentum mode measured can be read off the 3d-plot at the bottom of each panel. In general we observe a relatively smooth variation of all large momentum modes of the propagator across the phase transition in agreement with previous expectations [19].

These modes behave similar for SU(2) and SU(3). Only in the infrared some more drastic variations can be seen. These appear to be systematic close to the phase transition temperature and are somewhat more pronounced for SU(3). Although these variations are clearly not statisti-

cal in nature, it is not clear whether they are genuine. In particular, they may be volume effects, since increased long-wavelength thermal fluctuations close to the phase transition are not faithfully represented by the volumes presently employed. This possibility is supported by the fact that the effect is stronger in the case of SU(3) than of SU(2) where the employed volumes are smaller. In any case, more refined and systematic studies are necessary to explore the nature of these variations.

In general we observe that the chromomagnetic, transverse sector of Yang-Mills theory shows no pronounced reaction to the phase transition. The only essential effect is that with increasing temperature the propagator becomes stronger infrared suppressed and develops even a maximum at $p \approx 0.5$ GeV for the largest temperatures investigated here. This is indeed expected given that the propagator in the infinite-temperature limit of the dimensionally reduced theory in this gauge exhibits a clear maximum [39].

The situation is rather different for the chromoelectric, longitudinal part D_L of the gluon propagator, shown in figure 2. From the plots it is immediately visible that the longitudinal gluon reacts strongly to the phase transition, in accordance with previous observations [19]. For temperatures below the phase transition we observe a dramatic increase of the infrared part of the propagator close to the phase transition which leads to an even more dramatic decrease shortly above T_c . Also this dramatic variation seems to be more pronounced in the SU(3) data. This behaviour is most easily visible from the electric screening mass

$$m_L = D_L(p \rightarrow 0)^{-1/2},$$

and its associated susceptibility

$$\chi_T = \frac{\partial m_L}{\partial T},$$

which are shown in figure 3. This mass drops when moving towards the phase transition, reaches a minimum at the phase transition, and then quickly increases. In fact, the sensitivity is sufficiently strong that the gauge-invariant critical temperature can be determined independently from the chromoelectric screening mass just by extracting it from the plot. Indeed, this temperature coincides with the independently determined one using the Polyakov loop as an order parameter [37,38] within the resolution of the temperature grid employed here.

In the middle panel of figure 3 we zoom into the temperature region around the phase transition. From the available data, it appears that the screening mass in the SU(3) case is changing more rapidly across T_c than for the SU(2) case. It may be that this more rapid change signifies the first-order nature of the SU(3) transition, whereas in the SU(2) case the behavior is smoother as may be expected for a second-order phase transition, despite the larger physical volumes. This interpretation may also be supported by the much larger susceptibility in the SU(3) case, shown in the lower panel of figure 3. However, at present this interpretation may only indicate a possible

scenario and certainly has to be checked in a more detailed analysis [40]. In addition, a careful volume study is needed to check for the presence of long range correlations in the form of a vanishing electric screening mass of the SU(2) gluon at T_c .

Together, our results for the chromoelectric and chromomagnetic part of the gluon propagator indicate that the dominant response to the phase transition occurs in the chromoelectric sector. This finding can be related to the behaviour of certain dimension-two condensates [41,42]. These condensates are effectively given by the difference between the traces of the transverse and the longitudinal gluon propagator [33]. Thus the asymmetry observed in these condensates at finite temperatures [41] can be attributed essentially to the behavior of the longitudinal gluon propagator alone.

These comments complete our investigation of the temperature dependent gluon propagator. In the next section we will see that the gluon data are an important input into the Dyson-Schwinger equation for the quark propagator and therefore serve as a basis for our investigation of the order parameters for the chiral and deconfinement transition of quenched QCD.

3 Order parameters extracted from the quark propagator

3.1 The conventional and the dual quark condensate

The temperature dependent general expression for the inverse quark propagator S^{-1} is given by

$$S^{-1}(\mathbf{p}, \omega_p) = i\gamma_4 \omega_p C(\mathbf{p}, \omega_p) + i\gamma_i p_i A(\mathbf{p}, \omega_p) + B(\mathbf{p}, \omega_p), \quad (2)$$

with vector and scalar quark dressing functions C, A, B . A further tensor component proportional to $\sigma_{\mu\nu}$ is possible in principle but is negligible in the presence of a pure vectorial quark-gluon vertex [21], as used here. The momentum arguments are given in terms of the three momenta \mathbf{p} and generalised Matsubara frequencies ω_p

$$\omega_p(n_t, \varphi) = (2\pi T)(n_t + \varphi/2\pi). \quad (3)$$

These correspond to $U(1)$ valued boundary conditions for the quark fields, i.e. $\psi(1/T, \mathbf{x}) = e^{i\varphi} \psi(0, \mathbf{x})$. The angle φ varies between $\varphi \in [0, 2\pi[$, with $\varphi = 0$ for periodic and $\varphi = \pi$ for the usual, physical antiperiodic boundary conditions for the fermionic quarks.

Given the momentum behaviour of the non-perturbative dressing functions C, A, B one can extract a φ -dependent quark condensate from the propagator according to

$$\langle \bar{\psi} \psi \rangle_\varphi = Z_2 N_c T \sum_{\omega_p(\varphi)} \int \frac{d^3 p}{(2\pi)^3} \text{tr}_D S(\mathbf{p}, \omega_p(\varphi)). \quad (4)$$

The conventional quark condensate is obtained for the special case $\varphi = \pi$ and multiplication of this expression with

Z_m . In the limit of vanishing bare quark masses it is an order parameter for the chiral phase transition.

The corresponding dual observable, the dual quark condensate or dressed Polyakov loop, is obtained by a Fourier-transform of the φ -dependent condensate with respect to the winding number n ,

$$\Sigma_n = \int_0^{2\pi} \frac{d\varphi}{2\pi} e^{-i\varphi n} \langle \bar{\psi}\psi \rangle_\varphi \quad (5)$$

and specialising to the case $n = 1$. The dressed Polyakov loop Σ_1 is sensitive to the breaking and restoration of center symmetry [9,7] and therefore serves as an order parameter for the deconfinement transition.

These two order parameters, Eq. (4) with $\varphi = \pi$ and Eq. (5), can be extracted from the dressed, temperature dependent quark propagator calculated from functional methods as detailed in Refs. [13,14,17]. In the following we will update the calculation presented in Ref. [14] and in addition also extend the studies to the case of the gauge group SU(3). We will investigate whether and how the better temperature resolution of the lattice data for the gluon propagator discussed in the previous section leads to improved results for the order parameters. We also compare the results obtained for gauge group SU(2) and SU(3).

3.2 Truncation scheme for the Dyson-Schwinger equations for the quark propagator

The Dyson-Schwinger equation for the quark propagator at finite temperature T is given by

$$\begin{aligned} S^{-1}(\mathbf{p}, \omega_p) &= Z_2 S_0^{-1}(\mathbf{p}, \omega_p) - C_F \frac{Z_2 \tilde{Z}_1}{\tilde{Z}_3} g^2 T \sum_{n_k} \int \frac{d^3 k}{(2\pi)^3} \\ &\times \gamma_\mu S(\mathbf{k}, \omega_k) \Gamma_\nu(\mathbf{k}, \omega_k, \mathbf{p}, \omega_p) \\ &\times D_{\mu\nu}(\mathbf{p} - \mathbf{k}, \omega_p - \omega_k). \end{aligned} \quad (6)$$

Here $D_{\mu\nu}$ denotes the (transverse) gluon propagator in Landau gauge and we have introduced a reduced quark-gluon vertex Γ_ν , by defining $\Gamma_{\nu,i}^{full} = ig \frac{\lambda_i}{2} \Gamma_\nu$. The bare quark propagator is given by $S_0^{-1}(p) = i\gamma \cdot p + Z_m m(\mu^2)$, where $m(\mu^2)$ is the renormalized current quark mass. The wave function and quark mass renormalization factors, Z_2 and Z_m , are determined in the renormalization process. The ghost renormalization factor \tilde{Z}_3 is canceled by a corresponding factor in our model for the quark-gluon vertex discussed below. Furthermore we used $\tilde{Z}_1 = 1$ for the renormalization factor of the Landau gauge ghost-gluon vertex. The quark dressing functions $A(\mathbf{p}, \omega_p)$, $B(\mathbf{p}, \omega_p)$ and $C(\mathbf{p}, \omega_p)$ can be extracted from Eq. (6) by suitable projections in Dirac-space.

In Eq. (6) the Casimir factor $C_F = (N_c^2 - 1)/(2N_c)$ stems from the color trace. For $N_c = 2$ these equations have been solved numerically in Refs. [13,14] in a truncation scheme which used lattice results from Ref. [19] for the temperature dependent gluon propagator as input. As

discussed in the previous section we now have updated and refined results for the SU(2) and SU(3) gluon propagator at our disposal. These will be used in the following to provide for improved results for the quark propagator and the associated conventional and dual condensates.

In the Dyson-Schwinger equation (6) for the quark propagator we need to evaluate the gluon propagator at values of momentum which are not identical with the ones extracted on the lattice. In particular we need to evaluate the gluon at momenta larger than available lattice momenta. As it turns out, it is possible to use our knowledge on the analytical form of the gluon dressing functions $Z_{T,L}$ at zero temperature [43] to devise a fit function which is capable to nicely interpolate and extrapolate the lattice data also at finite temperature. These fits for the transverse and longitudinal dressing functions $Z_{T,L}$ of the gluon propagator are given by

$$\begin{aligned} Z_{T,L}(\mathbf{q}, \omega_q, T) &= \frac{q^2 \Lambda^2}{(q^2 + \Lambda^2)^2} \left\{ \left(\frac{c}{q^2 + \Lambda^2 a_{T,L}(T)} \right)^{b_{T,L}(T)} \right. \\ &\quad \left. + \frac{q^2}{\Lambda^2} \left(\frac{\beta_0 \alpha(\mu) \ln[q^2/\Lambda^2 + 1]}{4\pi} \right)^\gamma \right\}. \end{aligned} \quad (7)$$

Here we find a temperature independent scale parameter $\Lambda = 1.4$ GeV and the coefficient $c = 11.5$ GeV². Furthermore $\beta_0 = 11N_c/3$ and $\gamma = -13/22$ in the quenched theory and we renormalize at $\alpha(\mu) = 0.3$.

The fit function Eq. (7) generalises the one used in Refs. [13,14], where the temperature dependent exponent $b_{T,L}(T)$ has been kept fixed, i.e. $b_{T,L}(T) = 2$. Since we now have more accurate lattice gluon data at our disposal we found it useful to relax this condition and thus provide an even better representation of the lattice data. One may speculate whether an irrational exponent $b_{T,L}(T)$ with the corresponding temperature dependent cut in the p^2 -plane signals quantitative changes also in the analytic structure of the gluon, as suggested in [24,25]. A detailed investigation of this aspect is relegated to further systematic studies [40].

In general our fits are optimised in particular in the mid-momentum regime, which is most important later on when we use them as input into the quark-DSE. The details for the fit parameters as well as plots of the fits for selected temperatures are relegated to appendix D. Here we only show the resulting electric and magnetic screening masses of the gluon as extracted from the infrared behaviour of our fit functions. These are compared to the corresponding lattice results in fig. 4. The fit quality is very satisfactory, except for the electric screening mass at the largest temperatures. Here the lattice results suffer mostly from systematic artifacts due to the restricted number of points in the time direction [19]. This may be reflected in the mismatch of the screening masses with the ones extracted from our fit. Indeed, one may even argue that the electric screening masses from the fits are more accurate in the large temperature regime since they nicely reproduce the expected proportionality of the screening mass with temperature, $m_L \sim T$, known from hard ther-

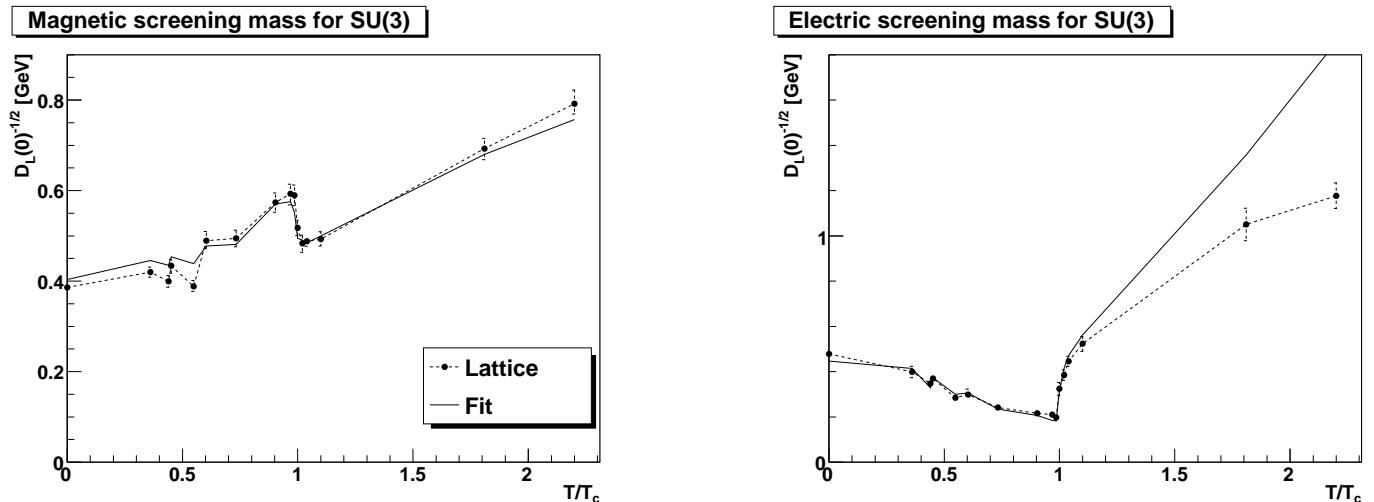


Fig. 4. Magnetic (left) and electric (right) temperature dependent scale parameters in our fits for the lattice gluon propagator compared with the lattice results for the magnetic and electric screening masses of the gluons.

mal loop results. We also note that at the two highest temperatures available the fit function describes the low and mid momentum behavior of the electric gluon propagator very precise. On the other hand the fit function Eq. (7) is not capable to describe the qualitative mid-momentum dependence of the magnetic propagator in this temperature range, as can be seen in fig. 9 in the appendix. We checked that this momentum behavior can be described precisely using in addition a momentum dependent screening term in the fit function. Anyway, in the important region around the critical temperature both fits work perfectly well and represent therefore a trustable input for the Dyson-Schwinger equation of the quark propagator.

Note that as a significant difference to the fits used in Refs. [13,14] it turns out that the transition of the electrical screening mass from its decreasing behaviour below the critical temperature T_c to the increase above T_c is much sharper than the one extracted in Refs. [13,14]. This sharp change around T_c was not resolved by the then available lattice data of Ref. [19]. As a consequence of the much improved temperature resolution available now we will see that the corresponding deconfinement transition extracted from the quark propagator is also much more pronounced than the one seen in [13,14]. This will be discussed in more detail in the next section.

The remaining piece to be specified in the quark-DSE is the dressed quark-gluon vertex. Similar to Refs. [13,14] we employ the following temperature dependent model

$$\Gamma_\nu(q, k, p) = \tilde{Z}_3 \left(\delta_{4\nu} \gamma_4 \frac{C(k) + C(p)}{2} + \delta_{j\nu} \gamma_j \frac{A(k) + A(p)}{2} \right) \times \left(\frac{d_1}{d_2 + q^2} + \frac{q^2}{\Lambda^2 + q^2} \right) \times \left(\frac{\beta_0 \alpha(\mu) \ln[q^2/\Lambda^2 + 1]}{4\pi} \right)^{2\delta}, \quad (8)$$

where $q = (\mathbf{q}, \omega_q)$ denotes the gluon momentum and $p = (\mathbf{p}, \omega_p)$, $k = (\mathbf{k}, \omega_k)$ the quark and antiquark momenta, respectively. Furthermore $2\delta = -18/44$ is the anomalous dimension of the vertex. Both together, the gluon dressing function and the quark-gluon vertex behave like the running coupling at large momenta; this is a necessary boundary condition for any model interaction in the quark DSE. The dependence of the vertex on the quark dressing functions A and C is motivated by the Slavnov-Taylor identity for the vertex; it represents the first term of a generalization of the Ball-Chiu vertex [44] to finite temperatures. The remaining fit function is purely phenomenological, see e.g. [45] where an elaborate version of such an ansatz has been used to describe meson observables. We use $d_2 = 0.5 \text{ GeV}^2$ for both gauge groups, but $d_1 = 7.6 \text{ GeV}^2$ for SU(2) and $d_1 = 4.6 \text{ GeV}^2$ for SU(3). The change in parameter d_1 from SU(2) to SU(3) is again motivated by the Slavnov-Taylor identity. At high temperatures it is expected that it reduces to the QED Ward-Takahashi identity multiplied with the non-perturbative ghost dressing function. A comparison of SU(2) and SU(3) ghost dressing functions in the infrared calculated on the lattice shows that for small momenta, $G(p)$ of SU(3) is reduced by roughly half compared to SU(2), see fig. 8. Even though the quantitative values for the ghost dressing functions at low momenta from the lattice might contain considerable uncertainties we assume the ratio of SU(2) to SU(3) to be reliable. In addition we also checked that a moderate variation of these parameters does not shift the critical temperatures of both, the chiral and the deconfinement transition.

Finally we wish to repeat a word of caution as concerns the chiral limit in our approximation scheme [14]. A prominent feature of the quenched theory not reproduced by our framework is the appearance of quenched chiral logarithms in the chiral condensate. These are well-known to be generated by η' hairpin diagrams, which are not represented by our vertex ansatz. For the present investigation we believe this is more an advantage than a drawback.

Quenched chiral logarithms are most notable in the chiral limit, where they lead to a singularity in the chiral condensate. Since we do not encounter this singularity we are in a position to investigate both, the ordinary condensate and the dressed Polyakov loop also in the chiral limit.

The numerical methods needed to solve the quark-DSE have been explained in detail in Ref. [14]. Having specified all necessary input we now proceed to present our results in the next subsection.

3.3 Numerical results

Our numerical results for the ordinary quark condensate, Eq. (4) with $\varphi = \pi$, and the dressed Polyakov loop, Eq. (5), are shown in Fig. 5. Let us first concentrate on the results for the ordinary quark condensate. Both, for SU(2) and SU(3) we find chiral transitions taking place on a very small temperature interval. This is particularly clear in the chiral limit (lower panel) but also for quark masses as heavy as the strange quark mass (upper panel). This temperature interval clearly coincides with the one identified in section 2.2 for the change of behaviour in the electric and magnetic screening masses. Technically what happens in the quark-DSE is that below T_c the electric, longitudinal part of the gluon propagator increases dramatically and therefore provides for extra interaction strength in the quark DSE. As a consequence, we find increasing values for the quark condensate. At or below T_c the electric part of the gluon propagator reaches its maximum and then drops sharply around and above T_c . In the quark-DSE this sudden loss of interaction strength is responsible for the dramatic decrease in the chiral condensate. It is satisfying to note that a similar behaviour has been observed from calculations of the quenched condensate via Casher-Banks relations on the lattice [46]. This agreement gives us confidence that the temperature dependence of our truncation for the quark-gluon vertex, Eq. (8), is at least qualitatively reliable and leads to meaningful results.

In the chiral limit we clearly obtain a chiral phase transition from the conventional quark condensate. Unfortunately, the temperature resolution of the lattice input is still not fine enough to unambiguously identify the order of the phase transition. One may speculate whether the SU(2) transition is second or first order, whereas the SU(3) one seems to be first order. The behaviour at finite quark masses may be compatible with a rapid cross-over for SU(2) and in the case of SU(3) even with a jump in the condensate signaling a remnant of a first order transition. Further investigations are necessary to clarify, whether the differences seen in Fig. 5 between SU(2) and SU(3) are indeed significant.

As concerns the dressed Polyakov-loop we clearly find a transition between the center-symmetric low temperature phase and the center-broken phase at transition temperatures very close to the ones encountered for the conventional quark condensate. Below T_c the dressed Polyakov-loop is almost constant and very small. For large quark masses close to the transition temperature we even find small negative values of the Polyakov-loop. We interpret

these as artifacts introduced due to mass dependencies in the quark-gluon vertex that are not represented by our vertex ansatz. At temperatures $T_c \leq T \leq 1.1T_c$ the Polyakov-loop rises sharply and then less steeply for larger temperatures. Within the temperature range investigated we do not yet see a saturation of the dressed Polyakov-loop at large temperatures, although the results in the chiral limit may bear some signals of such a behaviour. In general, the deconfinement transition extracted from the dressed Polyakov-loop is as pronounced as the corresponding signal in the electric and magnetic screening masses of the gluon propagator, discussed in section 2.2. Similarly to the chiral transitions, also here the temperature resolution and the systematic quality of the input gluon propagator is not yet good enough to cleanly identify an order of the deconfinement transition.

For SU(2), the results shown here replace previous ones reported in Refs. [13,14]. As already discussed above, the lattice data used as input in these works have been available only for four different temperatures and had to be interpolated in between. This procedure generated a smooth behaviour of the gluon propagator around the critical temperature resulting also in a broad transition range as concerns the chiral condensate. Here, with our much better temperature resolution as concerns the lattice gluon, we are able to identify this behaviour as an artifact of the interpolation procedure.

4 Summary

In this work we combined two non-perturbative methods, lattice calculations and functional methods using Dyson-Schwinger equations, in a common framework to play on their individual strengths and to reduce the inherent problems of each approach. In the lattice ab initio framework we determined the temperature behaviour of the electric and magnetic parts of the Landau gauge gluon propagator with fine enough temperature resolution to relate their behaviour to the critical temperatures of the deconfinement transition of Yang-Mills theory. For SU(2) and SU(3) we found a clear signal of the phase transition in the extracted electric screening mass and a less pronounced indication in the magnetic screening masses. We also verified the earlier expectations [19] that the 'bump' in the electric dressing function undergoes dramatic changes around T_c . These changes have been identified as the source of equally dramatic changes in the ordinary quark condensate as determined from the Dyson-Schwinger equation for the quark propagator: the condensate keeps rising below T_c only to decrease sharply at T_c . This behaviour is in agreement with previous observations from lattice calculations of the Casher-Banks relation [46]. It also locates the mechanism for chiral symmetry restoration in Landau gauge rather unambiguously in the (ultra-)soft electric sector of the theory, emphasizing its genuine non-perturbative nature.

As for the deconfinement transition we observe a clean transition from the dressed Polyakov-loop as determined from the Dyson-Schwinger equation for the quark propagator. The corresponding transition temperatures, $T_c \approx$

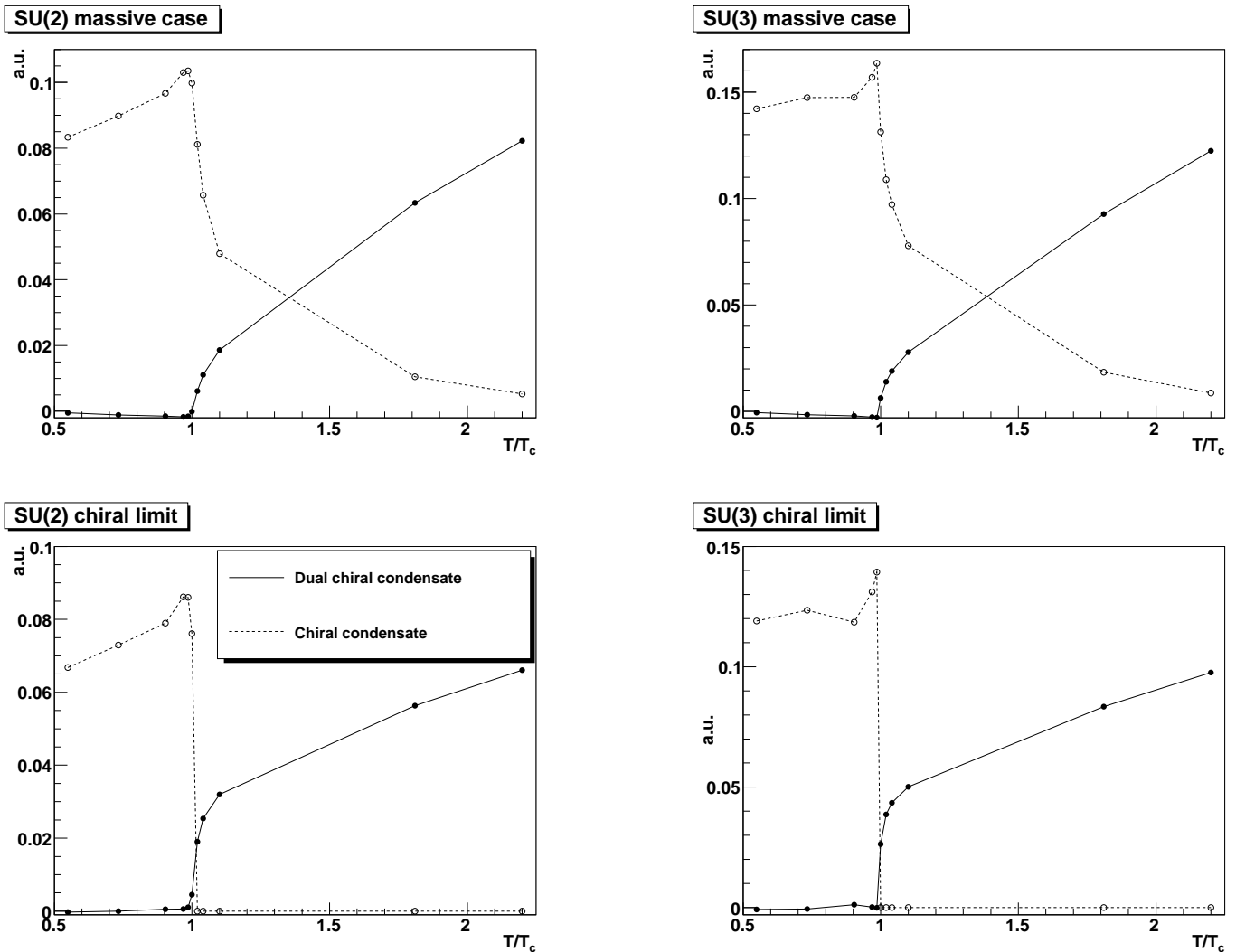


Fig. 5. The quark condensate $\langle \bar{\psi}\psi \rangle_\pi$ and the dressed Polyakov loop Σ_1 as a function of temperature for SU(2) (left panel) and SU(3) (right panel) Yang-Mills theory. Shown are results in arbitrary units (a.u.) for a massive (strange-)quark (upper panel) with $m \approx 80$ MeV and in the chiral limit (lower panel).

303 MeV for SU(2) and $T_c \approx 277$ MeV for SU(3) agree with the ones extracted from our lattice calculations. For SU(2) our results for the dressed Polyakov-loop update and refine the ones of Refs. [13,14], where only a much coarser lattice input for the gluon propagator has been available.

Finally we wish to emphasize that the dressed Polyakov-loop examined in our work is not the only gauge invariant order parameter for the deconfinement transition that can be calculated with functional methods. In Ref. [47] the Polyakov-loop potential has been determined within the functional renormalization group and delivered the expected first and second order phase transition for SU(3) and SU(2), respectively.

In general we believe that all these results demonstrate that combined efforts of the lattice and the functional framework provide a sound basis to determine gauge invariant observables in gauge fixed Yang-Mills theory. They also provide a good starting point to generalise the ap-

proach towards the inclusion of unquenching effects and the introduction of finite chemical potential.

Acknowledgments

We thank Lorenz von Smekal for helpful discussions. C. F. and J. M. were supported by the Helmholtz Young Investigator Grant VH-NG-332, by the Helmholtz Alliance HA216-TUD/EMMI and the Helmholtz International Center for FAIR within the LOEWE program of the State of Hesse. A. M. was supported by the FWF under grant number M1099-N16. Part of the computing time was provided by the HPC center at the Karl-Franzens-University Graz. The ROOT framework [48] has been used in this project.

A Simulation parameters and volume effects

In table 1 we present the simulation parameters for the lattice calculation of the temperature dependent gluon

Table 1. Data of the lattice gauge theory calculations as explained in the text.

Group	T/T_c	T [MeV]	N_t	N_s	β	a [fm]	$V_s^{1/3}$ [fm]	conf.
SU(2)	0	0	24	24	2.227	0.197	4.74	356
SU(3)	0	0	18	18	5.642	0.197	3.54	142
SU(2)	0	0	24	24	2.301	0.162	3.89	189
SU(3)	0	0	18	18	5.738	0.162	2.92	82
SU(2)	0.361	109	10	32	2.261	0.181	5.78	169
SU(3)	0.361	100	10	24	5.642	0.197	4.73	94
SU(2)	0.440	133	10	32	2.332	0.148	4.75	194
SU(3)	0.440	122	10	24	5.738	0.162	3.89	73
SU(2)	0.451	136	8	36	2.261	0.181	6.51	115
SU(3)	0.451	125	8	26	5.642	0.197	5.12	73
SU(2)	0.549	166	8	36	2.3315	0.149	5.35	152
SU(3)	0.549	152	8	26	5.738	0.162	5.12	79
SU(2)	0.603	182	6	40	2.262	0.180	7.21	140
SU(3)	0.603	167	6	30	5.642	0.197	5.91	62
SU(2)	0.733	222	6	40	2.332	0.148	5.93	326
SU(3)	0.733	203	6	30	5.738	0.162	4.86	64
SU(2)	0.903	273	4	46	2.2615	0.181	8.30	246
SU(3)	0.903	250	4	34	5.642	0.197	6.70	59
SU(2)	0.968	293	4	46	2.2872	0.168	7.75	256
SU(3)	0.968	268	4	34	5.675	0.184	6.16	63
SU(2)	0.986	298	4	46	2.2938	0.165	7.61	235
SU(3)	0.986	273	4	34	5.685	0.180	6.12	66
SU(2)	1.00	303	4	46	2.299	0.163	7.50	292
SU(3)	1.00	277	4	34	5.69236	0.178	6.05	65
SU(2)	1.02	308	4	46	2.306	0.160	7.35	280
SU(3)	1.02	282	4	34	5.7	0.175	5.95	67
SU(2)	1.04	314	4	46	2.313	0.157	7.21	319
SU(3)	1.04	288	4	34	5.71	0.171	5.81	113
SU(2)	1.10	333	4	46	2.333	0.148	6.80	276
SU(3)	1.10	305	4	34	5.738	0.162	5.51	71
SU(2)	1.81	548	2	52	2.263	0.180	9.35	232
SU(3)	1.81	500	2	38	5.642	0.197	7.49	59
SU(2)	2.20	665	2	52	2.332	0.148	7.71	310
SU(3)	2.20	609	2	38	5.738	0.162	6.16	70

propagator. The scale for SU(2) and SU(3) has been fixed according to [37] and [38], respectively, setting the string tension to $\sigma = (440\text{MeV})^2$, to which the considerations of [36] apply. T_c is then 303 MeV for SU(2) and 277 MeV for SU(3), at $\beta = 2.299$ and $\beta = 5.69236$, respectively, for the employed value of $N_t = 4$ at T_c . T is the corresponding temperature, N_t the temporal extent of the lattice, N_s is the spatial extent, β the bare coupling, a the lattice spacing and V_s the corresponding spatial physical volume. The number of configurations is denoted by conf., and the number of thermalization sweeps is given by $200 + 10N_s$, and of decorrelation sweeps by $20 + N_s$. Use has been made of the fact that the larger the number of generators, the less statistics is needed for the gluon propagator, due to the generator-averaging. The statistics was aimed at below the ten-percent 1σ statistical error level for the electric screening mass.

An imminent drawback for the comparison of SU(2) to SU(3) is the lower phase transition temperature of SU(3) in physical units. As a consequence, the already more expensive calculation for SU(3) would become even more ex-

pensive if the same physical volumes in spatial direction at a fixed time-extension would be required for SU(3). In this first investigation for SU(3), this has not been done, at the expense of larger finite-volume artifacts at low momenta for SU(3). These are exemplified in figure 6, where the results for the zero-temperature propagator for the smallest and largest discretization for SU(3) and SU(2) are compared, as an estimate for the systematic uncertainties involved. At finite temperature, the spatial volumes are larger, but in particular for the chromoelectric gluon this is counteracted by discretization artifacts [19].

B Soft vs. hard modes

At the temperatures studied here, functional studies suggest that the higher Matsubara frequencies can be approximated rather well by $D_T(\omega_p^2, \mathbf{p}^2) = D_T(0, \omega_p^2 + \mathbf{p}^2)$, and likewise for the other propagators [19,24]. That this is indeed a rather good approximation for the volumes employed here is shown in figure 7.

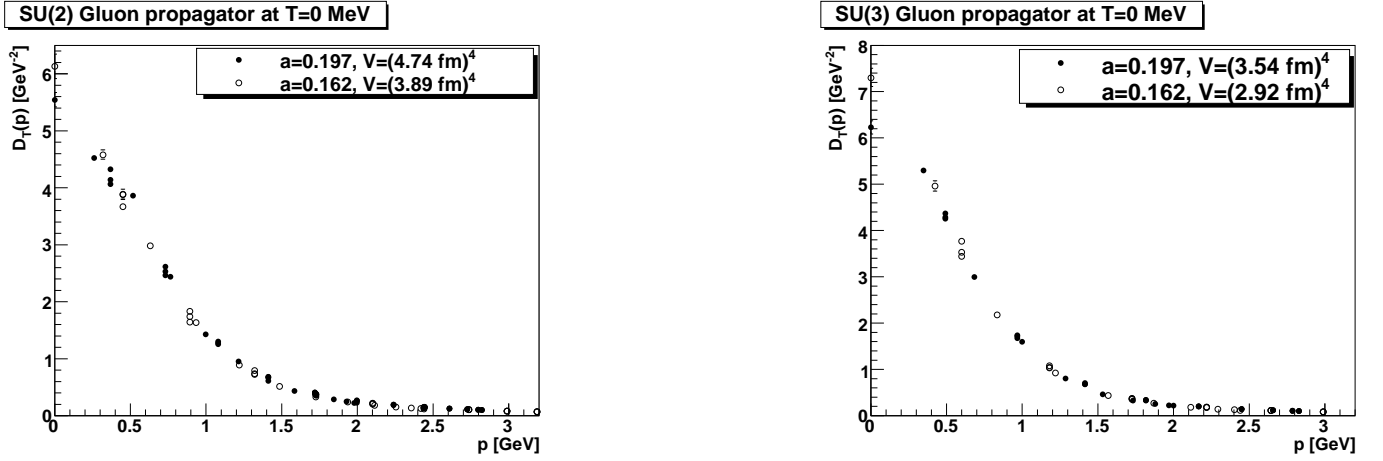


Fig. 6. The gluon propagator at zero temperature. SU(2) is shown in the left panel and SU(3) in the right panel.

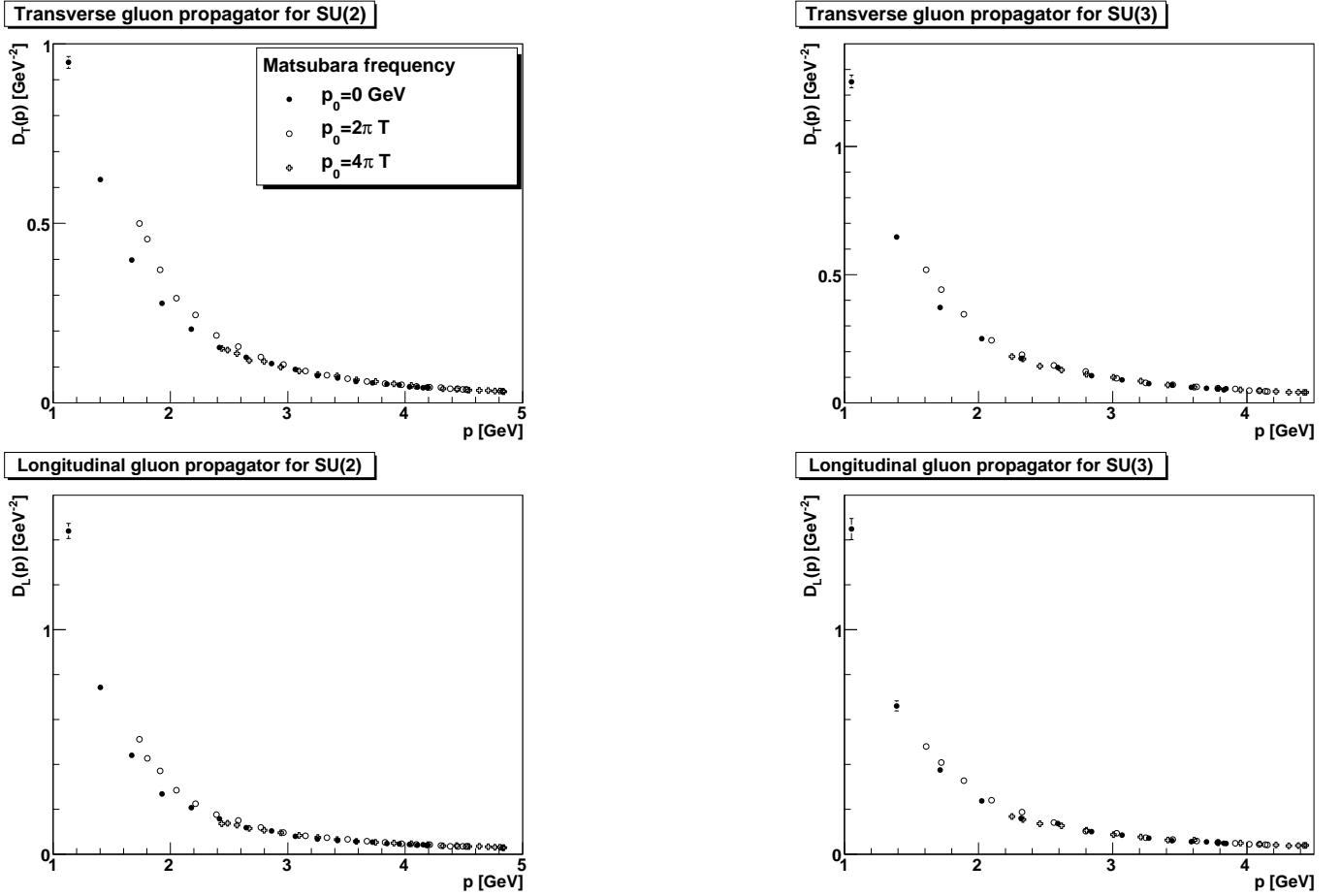


Fig. 7. Comparison of the soft mode to the first two higher Matsubara frequencies at $T = T_c$. In the upper panels the transverse gluon propagator is shown, and in the lower panel the longitudinal ones. In the left panels the results for SU(2) are compared to the results for SU(3) in the right panels. All results are shown as a function of the four momentum $p^2 = \omega_p^2 + (\mathbf{p})^2$.

C Ghost dressing function

The soft mode of the ghost is also associated with the chromomagnetic sector of the theory [19,24,25]. Consequently, in accordance with the expectation [19], it shows essentially no dependence on the temperature, see figure

8. If the ghost is indeed dominated by the gauge-fixing procedure this shows that the procedure is not affected significantly by a thermodynamic environment. The only observable effect, an increase in infrared strength with in-

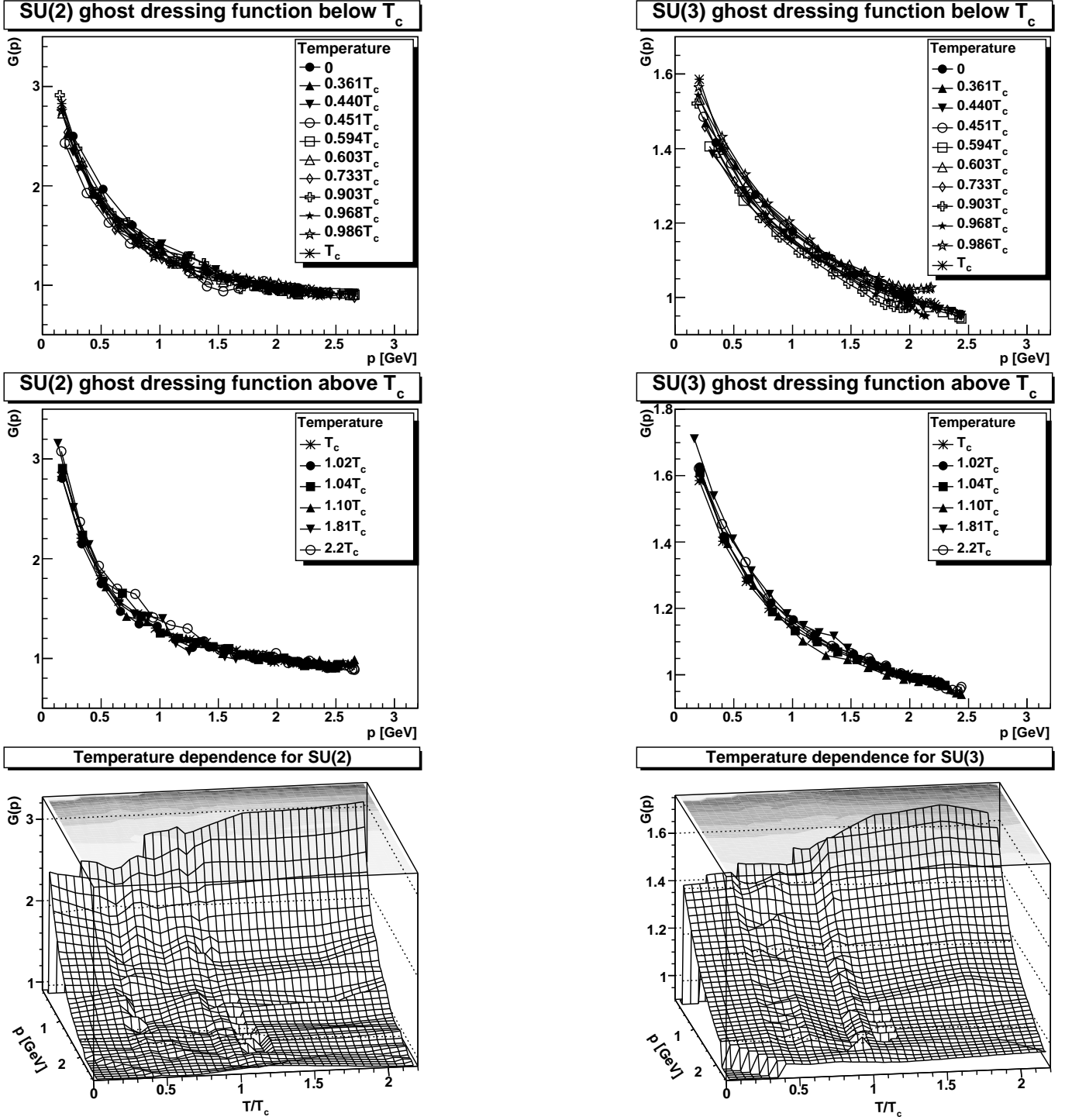


Fig. 8. The ghost dressing function $G(p) = p^2 D_G(p)$ of the ghost propagator D_G at temperatures below (top panel) and above (middle panel) the phase transition. The bottom panel shows both results together. On the left results for SU(2) and on the right results for SU(3) are shown. Lines are drawn to guide the eye.

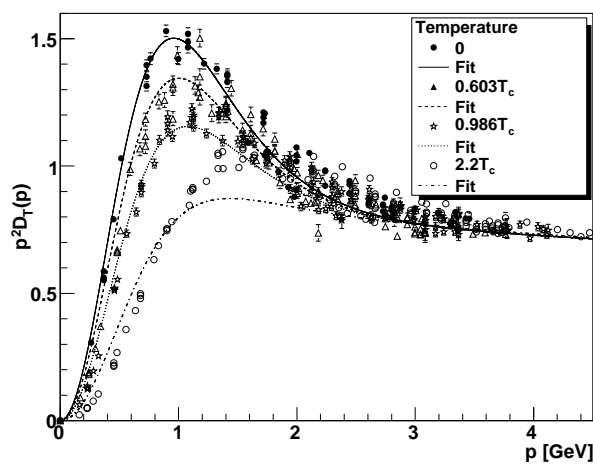
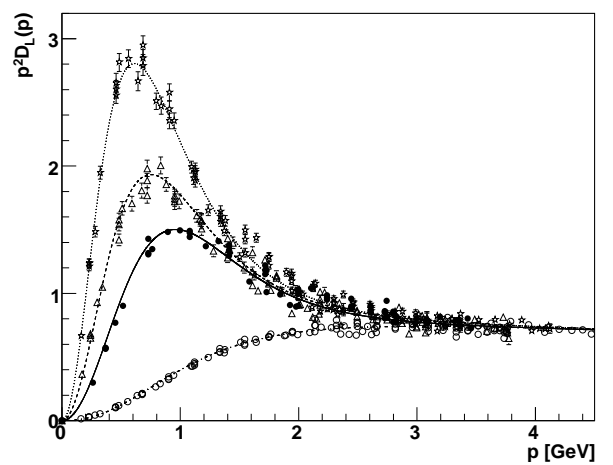
creasing temperature, is likely only an effect due to the larger spatial volumes used at higher temperatures.

D Fit functions for the temperature-dependent gluon propagator

As already detailed in the main body of this work around Eq. (7) we use a fit function for the temperature dependent

Table 2. Temperature dependent fit parameters for the SU(2) and SU(3) gluon propagator.

SU(2)																	
T/T_c		0	0.361	0.44	0.451	0.549	0.603	0.733	0.903	0.968	0.986	1	1.02	1.04	1.1	1.81	2.2
$a_L(T)$		1.22	0.62	0.48	0.63	0.30	0.29	0.21	0.15	0.15	0.15	0.18	0.34	0.56	0.93	2.69	5.00
$b_L(T)$		1.94	1.48	1.41	1.52	1.31	1.29	1.29	1.28	1.30	1.29	1.28	1.31	1.41	1.56	1.15	1.16
$a_T(L)$		1.22	1.31	1.31	1.39	1.31	1.32	1.32	1.33	1.32	1.29	1.24	1.26	1.30	1.37	1.33	1.35
$b_T(L)$		1.94	1.98	2.02	2.03	1.98	1.92	1.89	1.76	1.75	1.72	1.71	1.76	1.79	1.83	1.48	1.32
SU(3)																	
T/T_c		0	0.361	0.44	0.451	0.549	0.603	0.733	0.903	0.968	0.986	1	1.02	1.04	1.1	1.81	2.2
$a_L(T)$		0.60	0.42	0.23	0.33	0.19	0.17	0.11	0.098	0.082	0.079	0.16	0.27	0.32	0.50	2.71	4.72
$b_L(T)$		1.36	1.23	1.14	1.20	1.13	1.08	1.10	1.13	1.14	1.14	1.05	1.05	1.03	1.07	1.14	1.47
$a_T(T)$		0.60	0.71	0.78	0.83	0.86	1.04	1.05	1.67	1.57	1.06	0.54	0.55	0.57	0.63	1.47	1.42
$b_T(T)$		1.36	1.37	1.46	1.47	1.52	1.60	1.60	1.91	1.81	1.45	1.13	1.14	1.17	1.19	1.49	1.30

Comparison fit to data for SU(2)**Comparison fit to data for SU(2)****Fig. 9.** Magnetic (left) and electric (right) temperature dependent gluon dressing function from our lattice calculations compared with our fits.

longitudinal and transverse parts of the gluon propagator to represent the corresponding lattice data.

The resulting fit parameters $a_{T,L}(T)$ and $b_{T,L}(T)$ for the gauge groups SU(2) and SU(3) are given in tables 2. The rather good quality of the fits, given the statistical accuracy and systematic errors of the lattice calculations, can be seen in figures 4 and 9.

References

1. A. Bazavov *et al.*, arXiv:0903.4379 [hep-lat]; Y. Aoki, Z. Fodor, S. D. Katz and K. K. Szabo, Phys. Lett. B **643** (2006) 46 [arXiv:hep-lat/0609068].
2. M. Cheng *et al.*, arXiv:0911.2215 [hep-lat].
3. M. Cheng *et al.*, arXiv:0911.3450 [hep-lat].
4. Y. Aoki, S. Borsanyi, S. Durr, Z. Fodor, S. D. Katz, S. Krieg and K. K. Szabo, JHEP **0906** (2009) 088 [arXiv:0903.4155 [hep-lat]]; Y. Aoki, G. Endrodi, Z. Fodor, S. D. Katz and K. K. Szabo, Nature **443** (2006) 675 [arXiv:hep-lat/0611014].
5. F. Karsch and M. Lütgemeier, Nucl. Phys. Proc. Suppl. **73** (1999) 444. F. Karsch and M. Lütgemeier, Nucl. Phys. B **550** (1999) 449; J. Engels, S. Holtmann and T. Schulze, Nucl. Phys. B **724** (2005) 357 [arXiv:hep-lat/0505008].
6. F. Karsch and E. Laermann, arXiv:hep-lat/0305025.
7. E. Bilgici, F. Bruckmann, C. Gattringer and C. Hagen, Phys. Rev. D **77** (2008) 094007 [arXiv:0801.4051 [hep-lat]].
8. C. Gattringer, Phys. Rev. Lett. **97** (2006) 032003 [arXiv:hep-lat/0605018]; F. Bruckmann, C. Gattringer and C. Hagen, Phys. Lett. B **647** (2007) 56 [arXiv:hep-lat/0612020].
9. F. Synatschke, A. Wipf and C. Wozar, Phys. Rev. D **75** (2007) 114003 [arXiv:hep-lat/0703018]; F. Synatschke, A. Wipf and K. Langfeld, Phys. Rev. D **77** (2008) 114018 [arXiv:0803.0271 [hep-lat]].
10. E. Bilgici and C. Gattringer, JHEP **0805** (2008) 030 [arXiv:0803.1127 [hep-lat]].
11. J. Danzer, C. Gattringer and A. Maas, JHEP **0901** (2009) 024 [arXiv:0810.3973 [hep-lat]].
12. E. Bilgici, C. Gattringer, E. M. Ilgenfritz and A. Maas, JHEP **0911** (2009) 035 [arXiv:0904.3450 [hep-lat]].
13. C. S. Fischer, Phys. Rev. Lett. **103** (2009) 052003 [arXiv:0904.2700 [hep-ph]].
14. C. S. Fischer and J. A. Mueller, Phys. Rev. D **80** (2009) 074029 [arXiv:0908.0007 [hep-ph]].

15. E. Bilgici, F. Bruckmann, J. Danzer, C. Gatttringer, C. Hagen, E. M. Ilgenfritz and A. Maas, *Few Body Syst.* **47** (2010) 125 [arXiv:0906.3957 [hep-lat]].
16. W. Söldner, *PoS LAT2007* (2007) 222 [arXiv:0710.2707 [hep-lat]].
17. J. Braun, L. M. Haas, F. Marhauser and J. M. Pawłowski, arXiv:0908.0008 [hep-ph].
18. A. Roberge and N. Weiss, *Nucl. Phys. B* **275** (1986) 734; P. de Forcrand and O. Philipsen, *Nucl. Phys. B* **642** (2002) 290 [arXiv:hep-lat/0205016].
19. A. Cucchieri, A. Maas and T. Mendes, *Phys. Rev. D* **75** (2007) 076003 [arXiv:hep-lat/0702022].
20. R. Alkofer and L. von Smekal, *Phys. Rept.* **353**, 281 (2001) [arXiv:hep-ph/0007355]; C. S. Fischer, *J. Phys. G* **32** (2006) R253 [arXiv:hep-ph/0605173].
21. C. D. Roberts and S. M. Schmidt, *Prog. Part. Nucl. Phys.* **45** (2000) S1 [arXiv:nucl-th/0005064].
22. B. J. Schaefer and J. Wambach, *Phys. Part. Nucl.* **39**, 1025 (2008) [arXiv:hep-ph/0611191]; H. Gies, arXiv:hep-ph/0611146; J. M. Pawłowski, *Annals Phys.* **322**, 2831 (2007) [arXiv:hep-th/0512261].
23. I. Zahed and D. Zwanziger, *Phys. Rev. D* **61** (2000) 037501 [arXiv:hep-th/9905109].
24. A. Maas, J. Wambach and R. Alkofer, *Eur. Phys. J. C* **42**, 93 (2005) [arXiv:hep-ph/0504019].
25. A. Maas, J. Wambach, B. Grüter and R. Alkofer, *Eur. Phys. J. C* **37**, No.3, 335 (2004) [arXiv:hep-ph/0408074].
26. A. Maas, arXiv:0911.0348 [hep-lat].
27. S. Furui and H. Nakajima, *Few Body Syst.* **40**, 101 (2006) [arXiv:hep-lat/0612009].
28. A. Cucchieri, A. Maas and T. Mendes, *Phys. Rev. D* **74**, 014503 (2006) [arXiv:hep-lat/0605011].
29. F. Karsch and J. Rank, *Nucl. Phys. Proc. Suppl.* **42**, 508 (1995).
30. A. Cucchieri, F. Karsch and P. Petreczky, *Phys. Lett. B* **497**, 80 (2001) [arXiv:hep-lat/0004027]; *Phys. Rev. D* **64**, 036001 (2001) [arXiv:hep-lat/0103009].
31. A. Cucchieri and T. Mendes, *Nucl. Phys. B* **471**, 263 (1996) [arXiv:hep-lat/9511020];
32. A. Maas, arXiv:0907.5185 [hep-lat].
33. A. Maas, *Phys. Rev. D* **79** (2009) 014505 [arXiv:0808.3047 [hep-lat]].
34. I. L. Bogolubsky, E. M. Ilgenfritz, M. Müller-Preussker and A. Sternbeck, *PoS LATTICE2009* (2009) 237 [arXiv:0912.2249 [hep-lat]]; I. L. Bogolubsky, V. G. Bornyakov, G. Burgio, E. M. Ilgenfritz, M. Müller-Preussker and V. K. Mitrjushkin, *Phys. Rev. D* **77** (2008) 014504 [Erratum-ibid. *D* **77** (2008) 039902] [arXiv:0707.3611 [hep-lat]].
35. P. J. Silva and O. Oliveira, *Nucl. Phys. B* **690** (2004) 177 [arXiv:hep-lat/0403026].
36. A. Maas and Š. Olejník, *JHEP* **0802** (2008) 070 [arXiv:0711.1451 [hep-lat]].
37. J. Fingberg, U. M. Heller and F. Karsch, *Nucl. Phys. B* **392**, 493 (1993) [arXiv:hep-lat/9208012].
38. B. Lucini, M. Teper and U. Wenger, *JHEP* **0401** (2004) 061 [arXiv:hep-lat/0307017].
39. A. Cucchieri, T. Mendes and A. R. Taurines, *Phys. Rev. D* **67** 091502 (2003) [arXiv:hep-lat/0302022].
40. A. Maas, work in progress.
41. M. N. Chernodub and E. M. Ilgenfritz, *Phys. Rev. D* **78** (2008) 034036 [arXiv:0805.3714 [hep-lat]].
42. D. Dudal, J. A. Gracey, N. Vandersickel, D. Vercauteren and H. Verschelde, *Phys. Rev. D* **80** (2009) 065017 [arXiv:0907.0380 [hep-th]].
43. R. Alkofer, W. Detmold, C. S. Fischer and P. Maris, *Nucl. Phys. Proc. Suppl.* **141**, 122 (2005) [arXiv:hep-ph/0309078]; *Phys. Rev. D* **70**, 014014 (2004) [arXiv:hep-ph/0309077].
44. J. S. Ball and T. W. Chiu, *Phys. Rev. D* **22** (1980) 2542.
45. C. S. Fischer and R. Williams, *Phys. Rev. D* **78** (2008) 074006, [arXiv:0808.3372 [hep-ph]].
46. P. V. Buividovich, E. V. Luschevskaya and M. I. Polikarpov, *Phys. Rev. D* **78** (2008) 074505 [arXiv:0809.3075 [hep-lat]].
47. J. Braun, H. Gies and J. M. Pawłowski, *Phys. Lett. B* **684**, 262 (2010) [arXiv:0708.2413 [hep-th]]; F. Marhauser and J. M. Pawłowski, arXiv:0812.1144 [hep-ph].
48. R. Brun and F. Rademakers, *Nucl. Instrum. Meth. A* **389**, 81 (1997);